CHARACTERIZATION OF LUNAR CRATERS USING M−CHI DECOMPOSITIONS OF MINI-RF RADAR DATA. R. Keith Raney[1], Joshua T.S. Cahill[1], G. Wesley Patterson[1], D. Benjamin J. Bussey[1], and the Mini-RF Team. [1]JHU-APL, Laurel, MD (Keith.Raney@jhuapl.edu).

Introduction: In traditional optical remote sensing studies, lunar impact crater materials that are considered to be immature or recently disturbed are optically bright relative to their surroundings. Over time this signature can be subdued due to space weathering in the upper microns of the surface, where optical data is sensitive. Radar can image these same deposits at depths scaled to a longer radar wavelength. This information is conventionally expressed using the circular polarization ratio (CPR), which can be ambiguous when characterizing ejecta blankets or looking for water-ice. The Mini-RF radar aboard NASA's Lunar Reconnaissance Orbiter [1] (2009-) is a hybrid dual-polarimetric [2, 3], a form of compact polarimetry [4] and specifically designed to further differentiate contexts such as these.

Mini-RF, together with its precursor, Mini-SAR, on India's lunar Chandrayaan-1 satellite [5] (2008-9), are the first polarimetric synthetic aperture radars (SAR) outside of Earth orbit. These radars offer the same suite of polarimetric information from lunar orbit as Earth-based radar astronomy [6-8], since both types of radars measure the 2x2 covariance matrix of the backscattered field. These data are represented through the classical Stokes parameters [9].

In traditional radar astronomy, the four Stokes parameters (S_1, S_2, S_3, S_4), lead to child products which are used individually, of which CPR and the degree of linear polarization are well known examples [10, 11]. In contrast, the same four Stokes parameters support matrix decomposition techniques that to date are relatively unknown in radar astronomy, although they are well established analysis tools in Earth-observing 3x3 (or 4x4) polarimertic data [12]. We adapt that method to our 2x2 matrix data.

Method: Decomposition depends on identifying two (or more) variables—*e.g.* entropy and *alpha*—which when used together classify backscattering characteristics of the observed scene [13]. This method leads to unambiguous differentiation of single bounce, double bounce, or randomly-polarized backscatter.

The degree of polarization, m, has long been recognized as the single most important parameter characteristic of a partially-polarized EM field [14] and is defined by

$$m = (S_2^2 + S_3^2 + S_4^2)^{1/2} / S_1 \qquad (1)$$

The close relationship between entropy and degree of depolarization (1-m) has been verified experimentally [15]. The degree of depolarization (1-m) is indicative of randomly-polarized backscatter, typically arising from radar-quasi-transparent volumetric materials, such as lunar regolith.

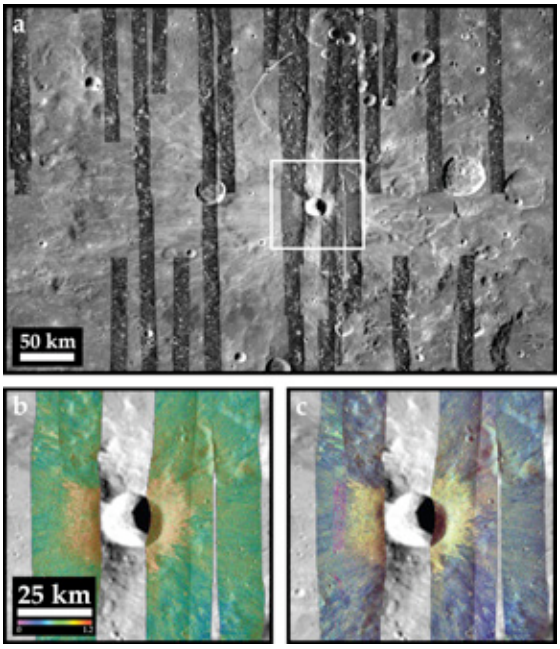

Figure 1. The crater Byrgius A is 19 km in diameter and located at 24.5°S, 63.7°W; (a) 100 m/pixel simple cylindrical LROC WAC image overlain with a Mini-RF S_1 data; (b) CPR information overlain on LROC WAC (bottom left); (c) *m-chi* decomposition overlain on LROC WAC.

For the Mini-RF radars, the Poincaré ellipticity parameter χ is the most robust choice for the second decomposition variable. It is one of the three principal components (m, χ, ψ) that are necessary and sufficient to describe the polarized portion of a partially-polarized quasi-monochromatic EM field of average strength S_1. Further, the sign of χ is an unambiguous indicator of even versus odd bounce backscatter, even when the radiated EM field is not perfectly circularly polarized, which is the case for the Mini-RF radar.

The Mini-RF team has adopted the *m−chi* decomposition as an analysis tool. In this formulation the key inputs are m, and the degree of circularity

$$\sin 2\chi = -S_4/mS_1 \qquad (2)$$

Then the *m−chi* decomposition may be expressed through a color-coded image, where

$$B = [mS_1(1 - \sin 2\chi)/2]^{1/2}$$
$$R = [mS_1(1 + \sin 2\chi)/2]^{1/2} \qquad (3)$$
$$G = [S_1(1 - m)]^{1/2}$$

Here, Blue indicates single-bounce (and Bragg) backscattering, Red corresponds to double-bounce, and Green represents the randomly polarized constituent.

Analysis and Discussion

Byrgius A – Physical Properties of Ejecta: Visible image data suggest that the 19 km diameter crater Byrgius A has an ejecta blanket that extends up to 300 km beyond its rim (**Fig. 1**). The extent of the blanket is observable in Mini-RF S_1 data as an increase in total backscatter with respect to the surrounding terrain (**Fig. 1a**). Derived CPR data clearly indicate the increased roughness associated with the continuous and discontinuous portions of the ejecta (**Fig. 1b**). An *m-chi* decomposition of the crater and its surroundings reveals the higher degree of double bounce backscatter and volumetric scattering associated with its ejecta (**Fig. 1c**). However, beyond the continuous portion of the ejecta blanket, we observe portions of surface covered by discontinuous ejecta in visible imagery that shows a predominance of Bragg scattering. This is not expected for ejecta material and is instead more indicative of the surrounding mature lunar regolith. The implication is that Mini-RF is illuminating material beneath the ejecta of Byrgius A. This suggests that the discontinuous blanket is relatively thin, on the order of a meter or less, since the backscattered wave's penetration can be no more than about ten wavelengths (12.6 cm at S-band). Such visibility through the ejecta blanket is not obvious in conventional radar or visible data. Characterization of such physical properties of the lunar surface is particularly important for identification of fundamentally different types of material (e.g., regolith, impact melt, etc.).

Goldschmidt – Looking for Water-Ice: Recent near-infrared spectral analyses of Chandrayaan-1's M^3, VIMS, and HRI-IR have presented compelling spectral evidence to confirm the presence of H_2O/OH on the Moon [16-18]. These data also suggest that H_2O/OH is not confined to permanently shadowed regions [17]. Lunar soils at the North Pole, such as within Goldschmidt crater, have enhanced near-infrared spectral absorptions suggestive of H_2O/OH, but the physical form and vertical distribution of H_2O/OH is still being debated [16, 19]. *Lawrence et al*. [20] have recently reexamined initial Lunar Prospector data evaluating a two-layer model (wet-over-dry) that is more consistent with the near-infrared results although still inconclusively attributed to hydrogen. If water ice is present within 0.1 cm – 1 meter vertical range, then there will be relatively high CPR ratios. However, in the context of evaluating the plausibility of water-ice, a high CPR result is somewhat ambiguous, particularly since high CPR can also suggest significant boulder populations and/or surface roughness.

In **Fig 2** mosaics of Anaxagoras and Goldschmidt craters data sets are shown. The bulk of the surface

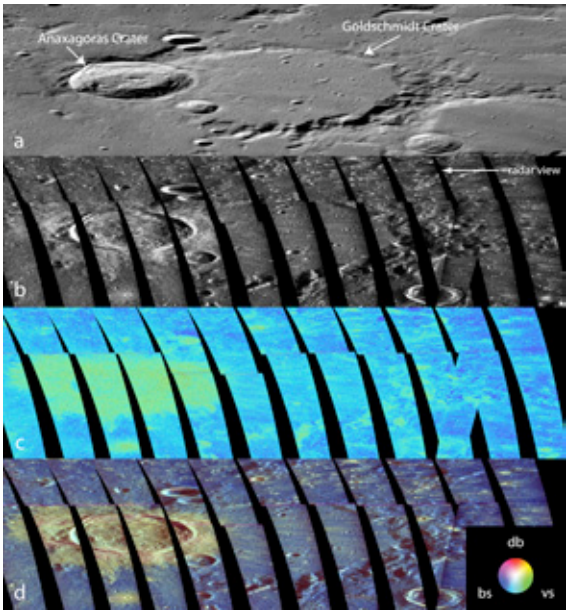

Figure 2. A 256 ppd simple cylindrical projection of the impact craters Anaxagoras and Goldschmidt shown in (a) LROC Wide Angle Camera monochrome image (b) total radar backscatter S_1, (c) circular polarization ratio (CPR), and (d) an *m−chi* decomposition

appears as blue in the *m−chi* image, suggesting smoothly comminuted, undisturbed surface soils. This is inconsistent with water-ice and indicates that Bragg backscattering (single-bounce) dominates the observed backscatter. In contrast, the impact crater Anaxagoras is an example of mixed scattering properties with an ejecta field appearing yellowish, indicating a mixture of volume and double-bounce backscattering.

Conclusions: Using the *m-chi* decomposition technique we demonstrate its utility to examine crater materials and the presence (or lack thereof) of coherent deposits of water-ice in the top meter of the lunar surface. This parameter also suggests the floor of Goldschmidt crater is consistent with single bounce Bragg scattering suggesting the absence of water-ice and further supporting adsorbed H to mineral grains or an H_2O frost as a plausible explanations for a H_2O/OH detection by near-infrared instruments.

References: [1] Chin *et al.*, *SSR* 129, 391 (2007); [2] Raney, in *Proceedings IEEE GRSS*. (IEEE, Denver, CO, 2006), ; [3] Raney, *IEEE TGRS* 45, 3397 (2007); [4] Nord *et al.*, *IEEE TGRS* 47, 174 (2009); [5] Goswami, Annadurai, *Current Science* 96, 486 (2009); [6] Raney *et al.*, *Proc. IEEE* 99, 808 (2011); [7] Stacy, Campbell, in *PGRSS IGARSS93*. (IEEE, Tokyo, Japan, 1993), pp. 30-33; [8] Carter *et al.*, *JGR* 109, E06009 (2004); [9] Stokes, *TCPS* 9, 399 (1852); [10] Carter *et al.*, *Proc. IEEE*, (2011); [11] Ostro, in *Solar System Remote Sensing Symposium*. (2002); [12] Cloude and Pottier, *IEEE TGRS* 35, 68 (1997); [13] Raney *et al.*, *JGR* (submitted), (2011); [14] Wolf, *Nuovo Cimento* 13, 1165 (1959); [15] Aiello, Woerdman, *PRL* 94, 1 (2005); [16] Pieters, *Science* 326, 568 (2009); [17] Clark, *Science* 326, 562 (2009); [18] Sunshine *et al.*, *Science* 326, 565 (2009); [19] Cheek, *JGR,* 116, (2011); [20] Lawrence *et al.*, *JGR,* 116, (2011);